Predicting the parabolic growth rate constant for high-temperature oxidation of steels using machine learning models

Aghaeian, S.; Nourouzi, F.; Sloof, W. G.; Mol, J. M.C.; Böttger, A. J.

DOI
10.1016/j.corsci.2023.111309

Publication date
2023

Document Version
Final published version

Published in
Corrosion Science

Citation (APA)
Aghaeian, S., Nourouzi, F., Sloof, W. G., Mol, J. M. C., & Böttger, A. J. (2023). Predicting the parabolic growth rate constant for high-temperature oxidation of steels using machine learning models. *Corrosion Science*, *221*, Article 111309. https://doi.org/10.1016/j.corsci.2023.111309

Corrosion Science 221 (2023) 111309

Contents lists available at ScienceDirect

Corrosion Science

journal homepage: www.elsevier.com/locate/corsci

Predicting the parabolic growth rate constant for high-temperature oxidation of steels using machine learning models

S. Aghaeian [a,*], F. Nourouzi [b], W.G. Sloof [a], J.M.C. Mol [a], A.J. Böttger [a]

[a] Department of Materials Science and Engineering, Faculty of Mechanical, Maritime and Materials, Delft University of Technology, Mekelweg 2, 2628 CD Delft, The Netherlands

[b] Department of Electrical Sustainable Energy, Faculty of Electrical Engineering, Mathematics and Computer Science, Delft University of Technology, Mekelweg 4, 2628 CD Delft, The Netherlands

ARTICLE INFO

Keywords:
A. Steel
B. Modeling studies
C. Oxidation
C. High-temperature corrosion
C. Kinetic parameters

ABSTRACT

The parabolic growth rate constant (k_p) of high-temperature oxidation of steels is predicted via a data analytics approach. Four machine learning models including Artificial Neural Networks, Random Forest, *k*-Nearest Neighbors, and Support Vector Regression are trained to establish the relations between the input features (composition and temperature) and the target value (k_p). The models are evaluated by the indices: Mean Absolute Error, Mean Squared Error, Root Mean Squared Error and Coefficient of Determination. The steel composition regarding Cr and Ni content and the temperature were the most significant input features controlling the oxidation kinetics.

1. Introduction

High-temperature oxidation occurs at different stages of steelmaking. The oxidation reaction can significantly influence the steel's properties, including the near-surface composition, wettability, corrosion performance, mechanical properties, etc. Therefore, knowing the oxidation behavior of the alloys is of great importance. Currently, evaluating the alloys' high-temperature oxidation occurs through lengthy and costly experimental trials. Hence, developing the capability of predicting the oxidation behavior of steels in a variety of conditions is highly desirable. Although analytical [1–3] and numerical [4–8] simulations have significantly improved the high-temperature oxidation investigations, they are usually applicable for specific material compositions or a given oxidizing condition such as exposure time and gas mixture composition.

Facing the limitations of the conventional modeling approaches in the field of materials science, together with recent improvements in machine learning (ML) techniques, open a pathway to the use of data analytics to predict the properties of materials [9–14]. Such algorithms have many advantages in providing insight into complex experiments on multi-component alloys. For instance, recent data analytics techniques in the design and development of new materials lead to a lower cost and can be considered as an alternative for experiments [13–15].

Despite the successful application of ML algorithms in the field of materials science, very limited studies addressed predicting high-temperature oxidation kinetics of alloys via data analytics approaches. In a recent work by Peng et al. [13] on NiCr-based alloys, a couple of different ML approaches have been applied to an experimental dataset to predict the parabolic growth rate constant (k_p) of oxidation. Alloy composition and temperature were the parameters, and k_p in both isothermal and cyclic oxidation was the target variable. The key input features were identified by Pearson's correlation coefficient (PCC) [16]. The oxidation temperature was found to have the biggest impact on the parabolic constant in all cases. It was also observed that Cr content, as the major alloying element in the studied alloys, had the most negative correlation with k_p, i.e. reduces the oxide growth kinetic constant. This agrees with previous studies, which showed that the presence of Cr promotes the formation of an external chromia solid-state diffusion barrier that slows down the oxidation reaction [17,18].

In another work by Bhattacharya et al. [14] ML algorithms were applied to predict the high-temperature oxidation kinetics of Ti alloys between 550 and 750 °C. The alloy composition, constituent phase of the alloy, the temperature of oxidation, time for oxidation, oxygen and moisture content, and mode of oxidation were considered as the independent input features, and k_p was set as the target value. When the Gradient Boosting Regressor algorithm [19] was employed, a good agreement was achieved between the experimental and the predicted k_p. Anirudh et al. [20] applied several ML models with a bottom-up approach (i.e. focussed on a very specific range of features) to predict the kinetics of elevated temperature cyclic oxidation of Fe-Cr and Fe-Cr-Ni alloys between 650 and 800 °C in 10% water vapor. The amount

* Corresponding author.
E-mail address: s.agheian@tudelft.nl (S. Aghaeian).

https://doi.org/10.1016/j.corsci.2023.111309
Received 20 January 2023; Received in revised form 26 May 2023; Accepted 2 June 2023
Available online 9 June 2023

of Ni and Cr, temperature, and time were considered the independent input features, while the mass change was the target value. In that case, CastBoost was found to give the best performance among all the ML models. On the other hand, in a work by Taylor et al. [15], oxidation kinetics for some grades of steels, as well as other corrosion-resistant alloys, were investigated via machine learning models with a top-down approach (i.e. including a large range of features). Therefore, the effects of many features including the wide range of composition, temperature, and gas environment were considered in the models. The models were applicable for more varied oxidizing circumstances since they had multiple features and a wide range for each, but they subsequently had substantial prediction errors. Finally, they found Ni, Cr, Al, and Fe to be the most significant elements controlling the oxidation kinetics.

Additionally, deep learning methods such as Artificial Neural Network (ANN) models have significantly influenced the development of materials and associated processes [21–27]. This is because these models can deal with complex problems in materials science, where the target value depends on a large number of variables. However, there are distinct patterns that knowledgeable metallurgists can recognize and comprehend. As shown by the work of Dewangan et al. [23] ANN is applicable to predict the oxidation kinetics of high entropy alloys (HEA). The composition of the alloys, oxidation time, and temperature were chosen as input parameters, while the mass gain of the oxidized sample was the output of the ANN model. Finally, it was shown that the ANN model predicts the high-temperature oxidation behavior of HEA in a consistent and precise manner. Kim et al. [24] analyzed the high-temperature oxidation resistance of Ni-based superalloys using the ANN model. Finally, although ML algorithms have been successfully applied for predicting the oxidation behavior of several alloys, there is very limited work on steels with a broad range of alloying element content.

Our literature review reveals no works on employing ML models for predicting oxidation kinetics for a variety of steel compositions, in air. Such high-temperature oxidation behavior is observed in the hot rolling process, which involves exposing heated sheets to air to cool down, which can have a substantial impact on the steel's performance and quality. In comparison to conventional steel development approaches based purely on limited experimental investigations or physical-based simulations, machine learning (ML) has the benefit of combining computational tools with experiments to forecast such oxidation behavior, having the potential to decrease development costs and time.

Here, a data analytics work is presented, which includes a correlation analysis of the high-temperature oxidation of a wide range of steels based on reported experimental data. In our work, the focus is on predicting the high-temperature oxidation kinetics of different steels, regardless of their phases, numerically represented by k_p. Because of having complex oxidation mechanisms, a broad, physics-based simulation of composition-dependent oxidation behavior is not yet feasible for steels. Correlation analysis was performed by PCC to find the interaction strengths between the input features (material and physical descriptors) and k_p statistically and rank them. Four widely used ML models were employed: Artificial Neural Network (ANN), Random Forest (RF), *k*-Nearest Neighbors (KNN), and Support Vector Regression (SVR). The performance of the models in predicting the k_p values was evaluated by different metrics and discussed.

2. Methods

2.1. Dataset

Most of the reported experimental works on high-temperature oxidation of steels, focus on the steady-state parabolic scaling kinetics where the oxide's growth rate is controlled by diffusion. Therefore, as a first step, a simple parabolic law (Eq. (1)) was chosen to describe the high-temperature oxidation kinetics

$$\left(\frac{\Delta m}{A}\right)^2 = k_p t \tag{1}$$

Table 1
List of the alloying elements range in wt%, oxidizing condition, and dataset details.

Steel composition	Fe (47.91–100), Mn (0–40), Cr (0–25), Al (0–14.33),C (0–0.82), Si (0–7.2), Ni (0–24.59), Cu (0–2.65), S (0–0.048), P (0–0.22)
Commercial grade	Crofer 22 APU, Crofer 22 H, SUS 310S, SUS 430, AISI 304, AISI 430, AISI 439, AISI 441, AISI 1018, HR3C, AFA, SIMP, FHSS, HSLA
Temperature, °C	500–1200
Atmosphere	Dry air
Input features	Elemental composition in wt%, and oxidation temperature
Target value, $g^2cm^{-4}s^{-1}$	Parabolic growth rate constant ($k_p = 3.2 \times 10^{-15}$–$1.21 \times 10^{-4}$)

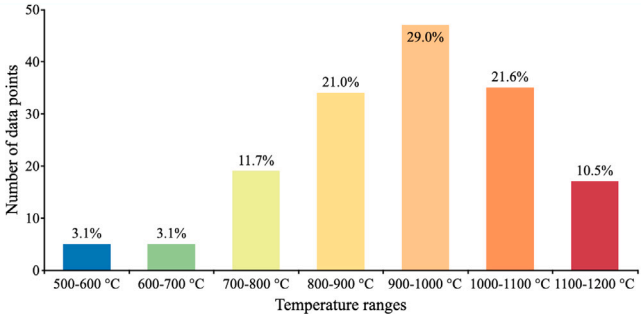

Fig. 1. Temperature distribution of the dataset between 500 and 1200 °C. The values on the bars show the portion of the data points in that range.

where Δm is the mass gain in g, A is the specimen surface area in cm^2, t is time in s, and k_p is parabolic oxidation constant in $g^2\,cm^{-4}\,s^{-1}$. Parabolic growth rate constants, k_p, were collected directly from published reports [3,28–56] where they were obtained from the mass gain results provided by Thermogravimetric analysis (TGA). The steps to get the parabolic growth rate constant are typically the same and begin with plotting the mass gain data on a squared mass gain vs. time plot. Then, a line is fitted to the linear part of the plot that represents the parabolic growth, and the slope of the fitted line would be the parabolic constant k_p. It is important to note that the dataset preparation was a manual literature survey to obtain values for k_p, without any extrapolation or interpolation. In this work, the focus is on the effect of steel composition and temperature (as input features) on oxidation kinetics k_p (target value). It is noted that data from the theoretical calculations were not included.

The collected dataset was tabulated for 76 different steel grades exposed to dry air at temperatures between 500 and 1200 °C. Within the data collection process, the dataset was visualized and studied at different stages to fill in the missing points. Finally, from a large amount of literature, 31 references were selected to prepare the dataset of 162 data points. It is not claimed to be a comprehensive dataset, but it will be shown later that it is enough to give precise quantitative predictions. The steel composition ranges, experimental conditions, and dataset details are shown in Table 1. The distribution of the dataset for temperature is shown in Fig. 1 as an example. The detailed information about the distribution of data for all of the features and the target value is depicted in Fig. A.1 and Fig. A.2, respectively in the appendix. To identify gaps in the experimental dataset and suggest experiments to improve model predictions, ML can ultimately be effectively merged with the automated design of experiment methods in future research.

Investigating the high-temperature oxidation of multi-component alloys and, specifically, steels is a complex process that requires information about the thermodynamics and kinetics of the reaction [57]. The parabolic growth rate constant (k_p) includes this information about

the material and conditions in high-temperature oxidation implicitly [13,14]. Such information encompasses the composition, temperature, gas mixture, etc. Since high-temperature oxidation in wet air has a different mechanism [57], only data for dry air has been collected for this work. ML algorithms utilize the collected data during the training process to predict the target value (k_p) for the testing data. However, the values for k_p were very small and it was difficult to visualize the differences between the calculated values. Therefore, by applying a logarithmic transformation (natural logarithm) of (k_p), the target value is converted. Therefore, the ML models in use will estimate the value of $\ln k_p$.

2.2. Correlation analysis and machine learning models

To identify the effect of each input feature on (k_p) and the interaction between different features, a PCC correlation analysis was conducted. PCC calculates the magnitude of the linear relationship between different features and allocates a value between 1 and −1. Positive and negative values, respectively, show a correlation and anti-correlation, while zero indicates no correlation. A correlation analysis facilitates the training of the ML model with the top-ranking features, which are the input features with the highest absolute value of correlation with the target.

The dataset was split into training and testing sets in a range of 60% to 95% and 40% to 5% of the dataset, respectively. As shown in Fig. A.3 in the appendix, smaller test sizes lead to high performances, but it is not reliable since the models are not tested with a sufficient number of data points and lead to unreproducible results. On the other hand, larger test sizes reduce the size of the training such that the reliability of the predictions is limited. A train and test size of respectively 80% and 20% were chosen as an optimum for reliable results. The data points were randomly distributed to the training and test sets by applying shuffling to the data before the split, which ensures the reproducibility of the results.

Four different models were employed to predict the parabolic growth rate constant (k_p): (a) Artificial Neural Network (ANN) [21], (b) Random Forest (RF) [58], (c) *k*-Nearest Neighbors (KNN) [59], and (d) Support Vector Machine (SVM) [60]. The regressor models of RF, KNN, and SVM were taken from Scikit-learn [61] sub-libraries to predict the continuous values of the target value (k_p). For ANN implementation, Keras was used, which is the high-level library built on top of TensorFlow [62]. Sequential and Dense models from the Keras library were used to add dense Neural Network layers. In addition, ReLU (Rectified Linear Unit) and Linear functions were employed respectively in hidden layers and the output layer.

In the KNN, the average number of neighbors for a given data point, or the *k*-nearest neighbors, is output by this non-parametric regression model. RF is a supervised learning technique that leverages the ensemble learning approach for regression. The ensemble learning method combines predictions from various ML algorithms (trees) to provide more accurate predictions than those from a single model. SVM is a powerful algorithm that allows choosing the tolerance of errors, both through an acceptable error margin (ϵ) and through tuning the tolerance of falling outside that acceptable error rate. Linear Regression (LR) [63] which is the most basic and commonly used predictive analysis algorithm was also employed in this work. It fits a linear equation to relate the input and output variables; however, the results are only described in the appendix due to lower accuracy.

To cover a wider class of ML algorithms, Artificial Neural Networks (ANNs) were used. ANNs are inspired by the biological nervous system and use interconnected mathematical nodes, also known as neurons, to describe complicated functional relationships. A typical ANN has input, hidden, and output layers. Building blocks of each layer are neurons that work as computational operation units. A neuron takes inputs from previous neurons, multiplies them by weights, and finally adds them up. Then this information is translated into output information by an activation function, and it can be used as input by other layers of neurons. This process is called feed-forward propagation, which generates the output layer. In addition, a back-propagation process is needed to update the weight values and improve system performance.

Other than training and test sets, in ANN there is a validation set that is different from the test dataset, and its role is to test the trained model but within the training phase. During training, the model is evaluated on the validation dataset after each epoch to see how well it is generalizing to new, unseen data. For the ANN model, the data points are randomly distributed between training, validation, and test data sets with a 0.6 : 0.2 : 0.2 ratio, respectively.

2.3. Evaluation of models

The ML models mentioned above were trained with different proportions of training data and by considering different numbers of top-ranking features found via PCC analysis. Then, the performance of each model was evaluated with four metrics [64]: (a) Mean Absolute Error (MAE), (b) Mean Squared Error (MSE), (c) Root Mean Squared Error (RMSE), and (d) Coefficient of Determination (R^2) (see Eqs. (2)–(5)),

$$R^2 = 1 - \frac{\sum_{k=1}^{n} \left(y_k - \hat{y}_k\right)^2}{\sum_{k=1}^{n} \left(y_k - \bar{y}\right)^2} \tag{2}$$

$$\mathrm{MSE} = \frac{1}{n} \sum_{k=1}^{n} \left(y_k - \hat{y}_k\right) \tag{3}$$

$$\mathrm{MAE} = \frac{\sum_{k=1}^{n} |\hat{y}_k - y_k|}{n} \tag{4}$$

$$\mathrm{RMSE} = \sqrt{\frac{\sum_{k=1}^{n} \left(\hat{y}_k - y_k\right)^2}{n}} \tag{5}$$

where y_k = measured k_p value, $\hat{y}_k$ = predicted k_p value, $\bar{y}$ = mean k_p value, and n = number of data points.

3. Result and discussion

3.1. Correlation analysis

The correlation coefficient between all the variables (input features and the target value) is presented in Fig. 2. While Fe content is the balance of the remaining alloying elements as the base element, it is important to note that Fe content is still utilized as an input feature because ML algorithms only solve mathematical problems and do not recognize this correlation. The last row and the last column of the matrix in Fig. 2 show the correlation between the features on the target value, and the absolute values show the magnitude of each feature's influence on the target value (see Section 2.2). The amount of Cr was identified to have the most significant negative impact on $\ln(k_p)$ among all the features. It was also found that the oxidation temperature had the second-highest impact on the target value. Fe and Ni were the third and fourth top-ranking features, respectively.

The findings from the correlation analysis were in agreement with the current oxidation knowledge [57]. For instance, it is known that increasing the amount of Cr in steels, promotes the formation of the external chromia solid-state diffusion barrier, which results in a slower oxidation reaction and a lower value of k_p [65,66], which is consistent with the big negative correlation value (−0.72) between Cr and $\ln(k_p)$. Moreover, iron produces rapidly forming oxides, and it has the highest positive correlation with $\ln(k_p)$ [67]. PCC also correctly identified that temperature has a high positive correlation with the target value (0.48). This is well-explained because increasing the temperature in the parabolic regime – which is known to be controlled by diffusion – can accordingly lead to higher k_p values [68]. It can also be observed in Fig. 2 that Ni has a large negative correlation with the target value. Such correlation, which is due to the formation of protective oxides, has

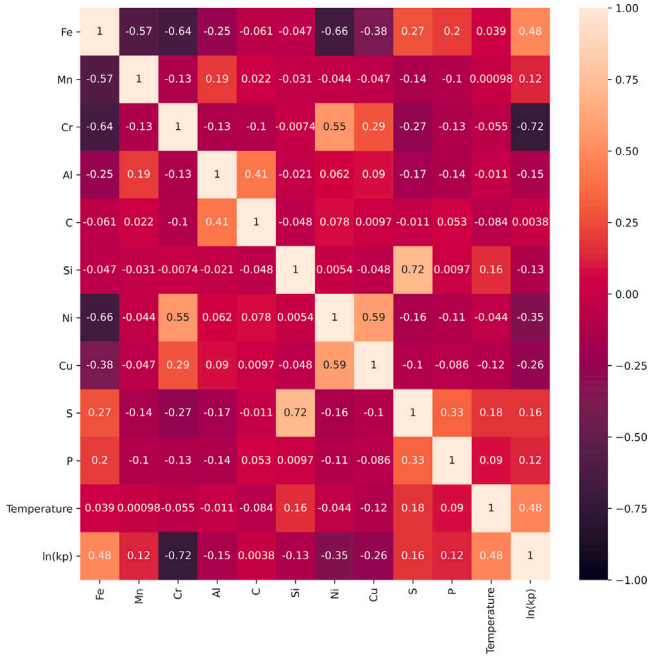

Fig. 2. Graphical representation of the correlation between the input features and $\ln(k_p)$ for the training set determined using the PCC method.

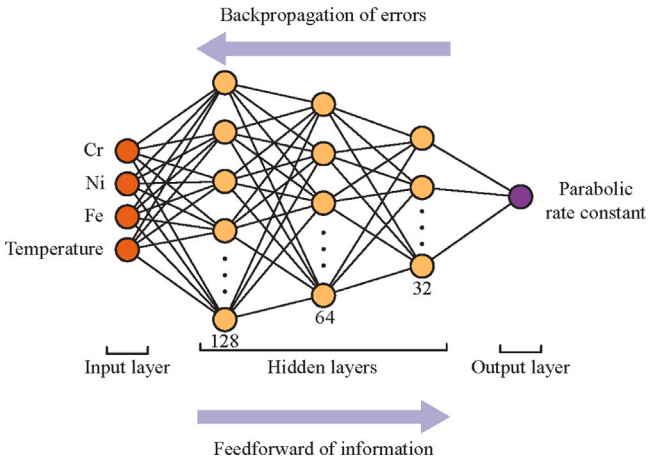

Fig. 3. Graphical view of the ANN model with the parameters used in this work.

Table 2
Performance comparison of ML models trained with four top-ranking features over the mean absolute error (MAE), mean squared error (MSE), root mean squared error (RMSE), and coefficient of determination (R^2).

	MAE	MSE	RMSE	R^2
RF	2.65	11.86	3.44	0.93
KNN	3.41	21.77	4.67	0.87
ANN	2.89	15.17	3.89	0.82
SVR	5.99	59.30	7.70	0.66

been seen and discussed before in the literature [20,57,67]. Moreover, the relative effect of the absolute correlation values of different features could also be analyzed. For instance, the bigger correlation value of Cr-$\ln(k_p)$ compared with temperature-$\ln(k_p)$ was in agreement with the results found in previous experimental [69] and machine learning [20] works.

The aim of this correlation study is not only to acquire information about how input features affect k_p, but also to implement it for finding the top-ranking input features for ML model training and to study the effect of this selection on model performance.

3.2. The performances of machine learning algorithms

Four different algorithms (ANN, RF, KNN, and SVM) are trained and their performances have been evaluated by four metrics of MAE, MSE, RMSE, and R^2. In each of the employed models, there are several hyperparameters that can be tuned. Some parameters such as the number of considered top-ranking input features, and the test/training dataset ratio are applicable for all of the employed models and can be optimized for each separately. However, each model can have its own specific hyperparameters as well. For instance, the number of trees in RF, the number of neighbors in KNN, or the number of hidden layers and nodes in ANN.

The final structure of ANN used in this study is shown in Fig. 3. It can be seen that the four top-ranking features are considered to be the input nodes. The developed ANN has one input layer with 4 neurons, three hidden layers with 128, 64, and 32 neurons, and an output layer with 1 neuron. The linear activation function with Adam optimizer [70] showed the best result in 1000 epochs [71]. An epoch is a hyperparameter that determines how many times the learning algorithm will run over the whole training dataset. Every sample in the training dataset has had a chance to update the internal model parameters once during an epoch.

The effect of the considered number of top-ranking features on the performance of each model is shown in Fig. 4. The top-ranking features are taken from the |PCC| ranking (the absolute values in Fig. 2). Results indicate that, to varying degrees, the models are sensitive to the number of considered features in training. ANN, RF, and KNN showed better performances by reaching $R^2 > 0.9$, while SVR could not surpass 0.7. Generally, increasing the number of considered top-ranking features to 3 increased the performances of the models significantly. For SVR and RF, considering more than 3 features did not considerably enhance the efficiency of the models. On the other hand, KNN and ANN reached maximum efficiency when using the top 7 to 10 features.

Furthermore, the different indices show approximately the same trends in terms of the number of features' influence on the performances. While R-squared (Fig. 4(d)) shows a clear difference in the precision of the models (RF>KNN>ANN>SVR), the other indices (Fig. 4(a), (b), and (c)) show a comparable performance for ANN, RF, and KNN. However, it is worth mentioning that the computational cost for models such as ANN is much more than SVR. In our work, the execution time for the models was measured in the code and the approximate ratio was 1 : 1 : 12 : 2671, for SVR, KNN, RF, and ANN, respectively. So, in (industrial) applications where the dataset is huge, the calculation time is an important parameter in choosing the most efficient model.

From Figs. 2 and 4, it is clear that employing just 3 features makes the predictions comparable to those made with all 11 features. In other words, adding features with lower PCC absolute values did not increase the accuracy of the predictions. Though, it is worth mentioning that such observation is only based on the prepared dataset which is made from the available experimental results on HT oxidation of steels. Therefore, the results are limited to the included range of features and not beyond that.

The performances of the employed ML models trained with four top-ranking input features are indicated in Table 2. Regarding all four indices, and for models trained with the four top-ranking features, RF and SVR had the best and the worst performances, respectively. It can be seen that ANN and KNN models show comparable performances evaluated via different indices. For instance, the R-squared value shows better performance of KNN compared with ANN, while the other indices show the opposite.

The training and validation losses over time for the ANN model are shown in Fig. 5. The training loss indicates how well the model is

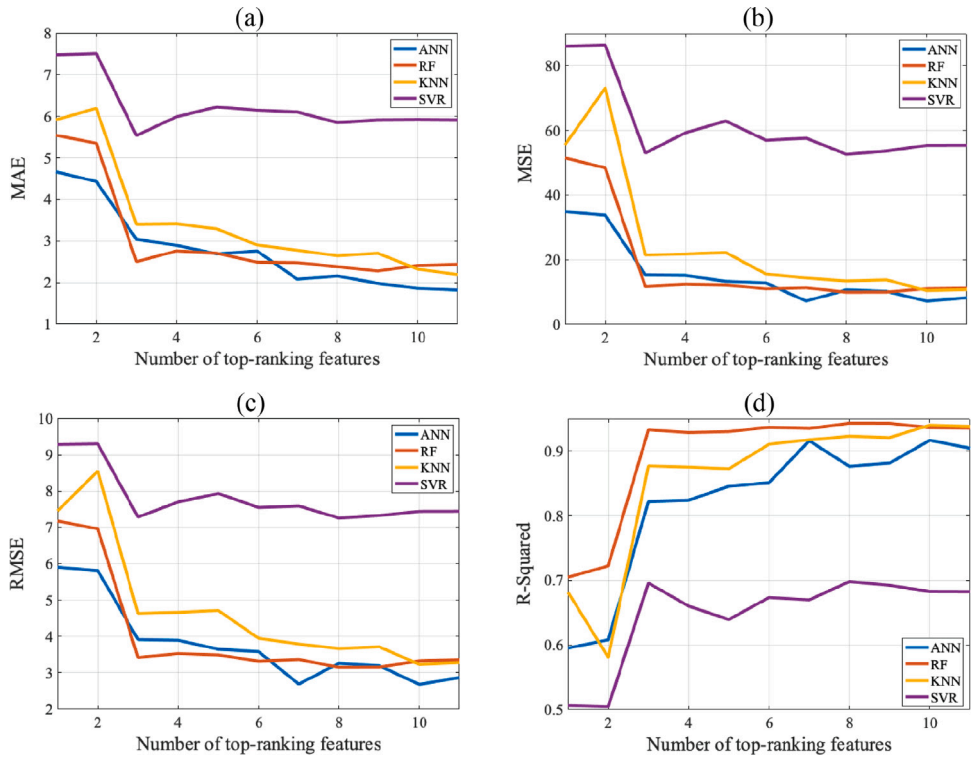

Fig. 4. The performances of the ML models (KNN, RF, SVM, and ANN) as a function of the number of top-ranking features evaluated by (a) MAE, (b) MSE, (c) RMSE, and (d) R-squared indices.

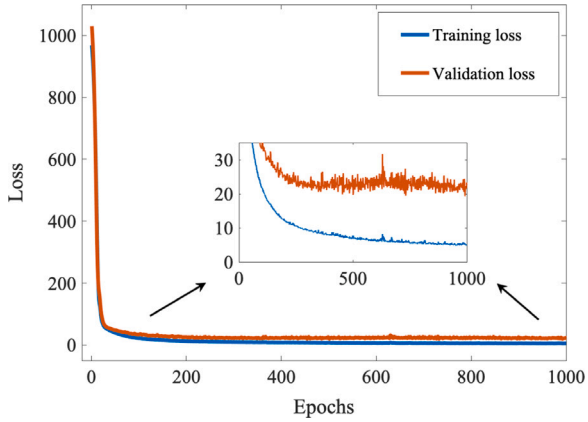

Fig. 5. Comparison of training and validation losses in ANN model.

fitting the training data, while the validation loss shows how well the model is adapting to the unseen data. The MAE metric is implemented to evaluate the performance of the ANN model by calculating the validation loss, and MSE is used to minimize the loss function and determine the training loss throughout the training process. It is shown that both losses are going down, which means that the predictions are good and the error is decreasing (no under-fitting). On the other hand, there is no divergence between the lines at longer times (higher epochs), and the validation loss does not increase, which shows that the ANN model is good at predicting the new data (no over-fitting).

For RF to perform at its best in this study, the top three features had to be included; after that, the performance was virtually completely independent of the number of features taken into account. The same trend was seen for the RF model in a previous work [13]. Such a trend is understandable because as an ensemble learning method, RF gives varied importance to each feature during model training; as a result, fewer important features would have less or even no contribution to its performance. This leads to a performance that is not sensitive to the number of features when the maximum accuracy is achieved.

The performances of all four models in predicting the target value for the testing data points when they were trained with four top-ranking features have been visualized in Fig. 6 . These plots show the comparison between the predicted and actual k_p values. The blue lines depict the case when the actual and predicted values are identical (perfect prediction), and the red dots are the testing dataset. All four graphs show the predicted results from models tested with 20% of the dataset, which means 32 data points. Therefore, having the red points close to the blue line means a good prediction for the models. It can be seen that all the models except SVR could reasonably predict the k_p for high-temperature oxidation of steels. Furthermore, RF is clearly generating more precise values for k_p. Similar to what was reported in Table 2, it can also be seen in Fig. 6 that the performances of ANN and KNN are relatively comparable. While R-squared shows slightly better results for KNN, the other indices show significantly lower errors in ANN predictions. Such a difference relates to the nature of the indices and the way that they calculate the errors [64] (see Eqs. (2)–(5)).

A general summarizing schematic of this data-driven work is shown in Fig. 7, from stating the problem to finalizing the predictions via the trained ML models.

4. Conclusion

The kinetic data (k_p) for high-temperature oxidation of a wide range of steel grades, regardless of their phases, in dry air was extracted from published data. Four different machine-learning models namely ANN, RF, KNN, and SVR were employed to predict k_p using the Phyton-libraries: Scikit-learn and TensorFlow. The models were evaluated by MAE, MSE, RMSE, and R-squared indices, and they were improved by optimizing the hyperparameters to get their best performance. The most significant features controlling the oxidation kinetics were the Cr, Fe, and Ni content as well as the temperature. Moreover, the models

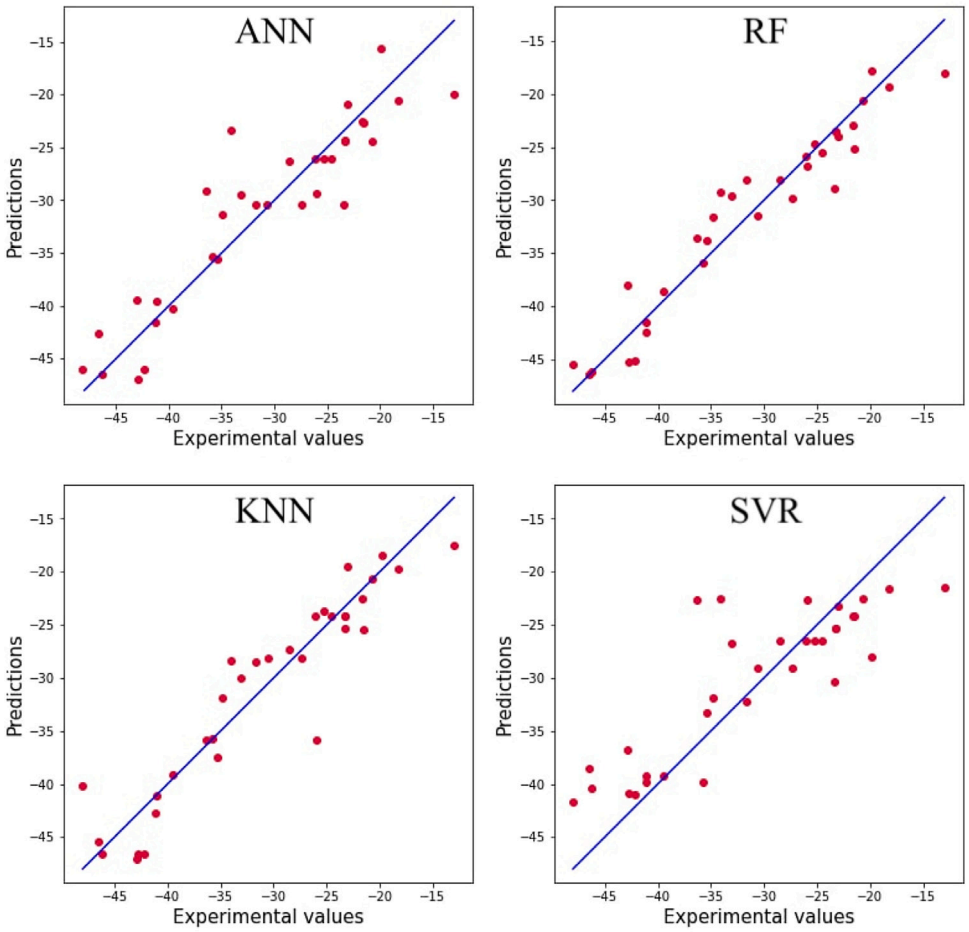

Fig. 6. Actual values of experimental parabolic growth rate constants of high-temperature oxidation compared with values obtained from the ML models (ANN, RF, KNN, and SVM), where all the models were trained with four top-ranking features and tested with 20% of the dataset (32 red dots).

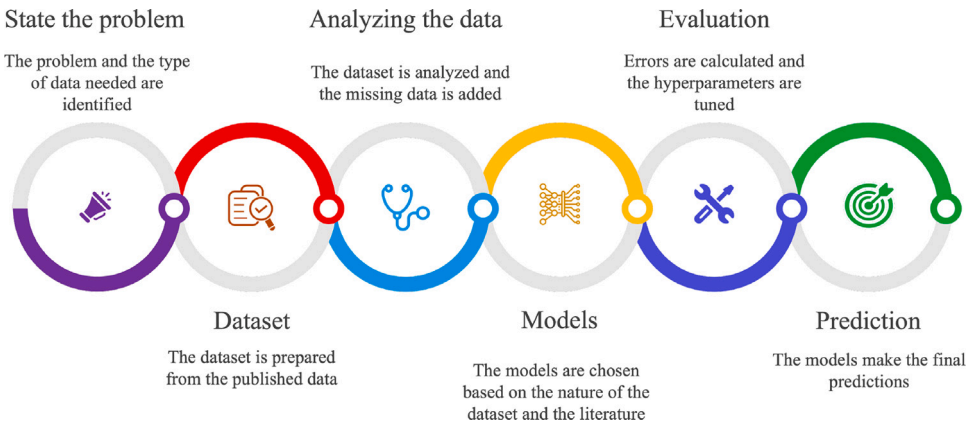

Fig. 7. A general schematic of the steps taken in this work.

could successfully establish the relationship between the input features (composition and temperature) and the target value (k_p). Finally, it was shown that including more than three features, did not significantly improve the ML predictions. However, when trained with four top-ranking features, RF was found to have the smallest error in predictions, while KNN and ANN were shown to have almost the same prediction accuracy. SVR showed the largest errors in predicting the target value. The knowledge gained from this work can be useful in predicting the oxidation behavior of newly designed steel grades at different steps of the steel-making process where high-temperature oxidation can happen. It is possible with the valuable quantitative information provided about the correlation values of different features. Furthermore,

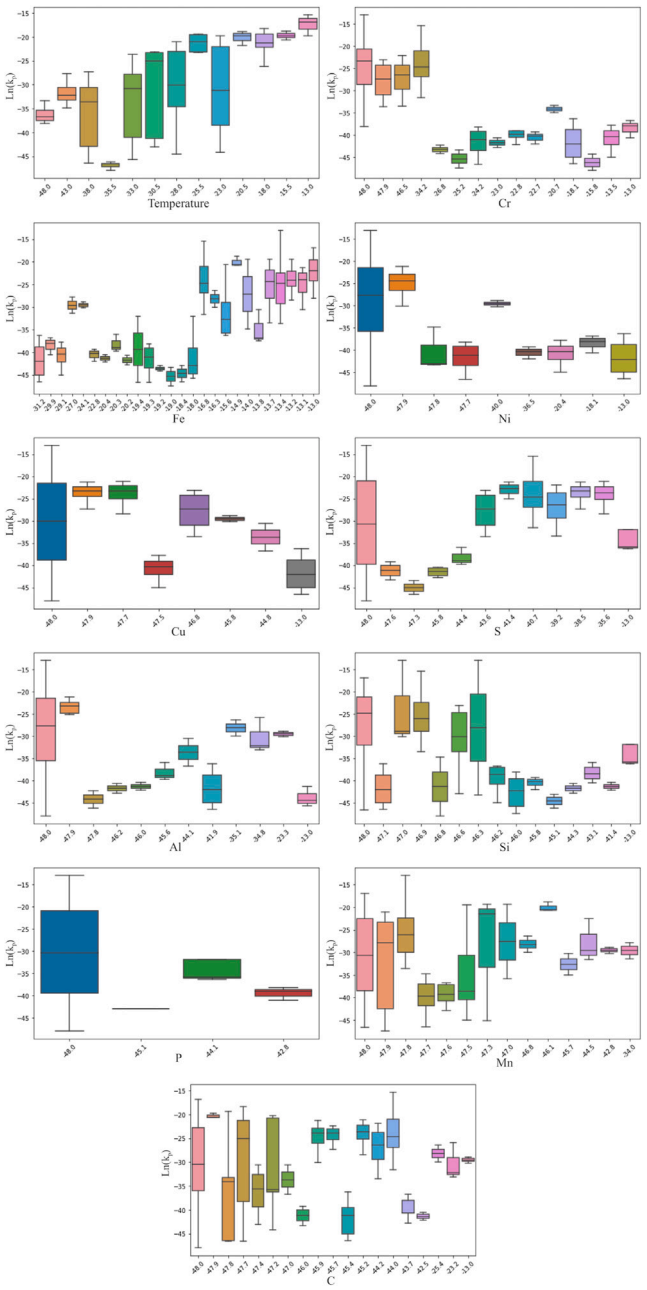

Fig. A.1. The distribution of the dataset for all the features. The X axes show the normalized values.

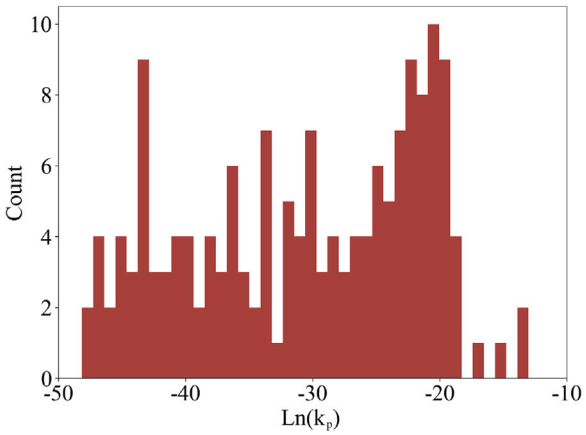

Fig. A.2. The distribution of k_p values in the dataset.

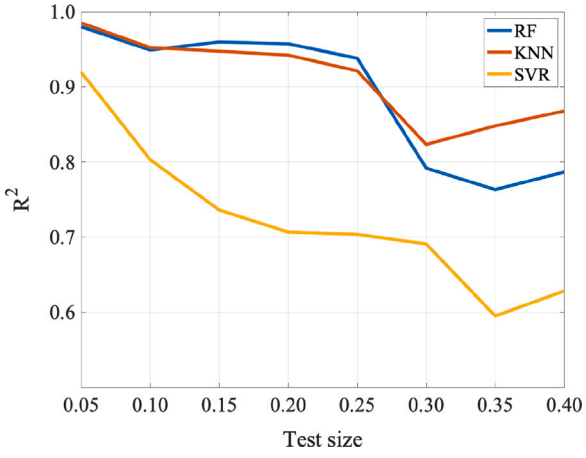

Fig. A.3. The R-squared error for RF, KNN, and SVR models as a function of the size of the test dataset. The models are trained with the remaining portion of the data which is the training dataset.

the described method can be applied to datasets for other alloys, or investigate the effect of other features such as the components of the gas environment and their partial pressures on the kinetics of oxidation. In the end, in order to discover gaps in the experimental dataset and suggest experiments to improve the model predictions even further, machine learning can be effectively integrated with the automated design of experiment techniques.

CRediT authorship contribution statement

S. Aghaeian: Conceptualization, Methodology, Software, Writing – original draft, Investigation. **F. Nourouzi:** Software, Validation, Data curation. **W.G. Sloof:** Writing – review & editing. **J.M.C. Mol:** Supervision, Writing – review & editing. **A.J. Böttger:** Supervision, Project administration, Funding acquisition, Writing – review & editing.

Declaration of competing interest

The authors declare that they have no known competing financial interests or personal relationships that could have appeared to influence the work reported in this paper.

Data availability

Data will be made available on request.

Acknowledgments

This work was supported by the research program of the Materials innovation institute, The Netherlands (M2i, www.m2i.nl) [project number T17019p], which is supported by the Dutch government. The authors are indebted to Dr. W. Melfo and Dr. P. J. van der Wolk of Tata Steel (IJmuiden, The Netherlands) for the valuable discussions.

Appendix

See Figs. A.1–A.5.

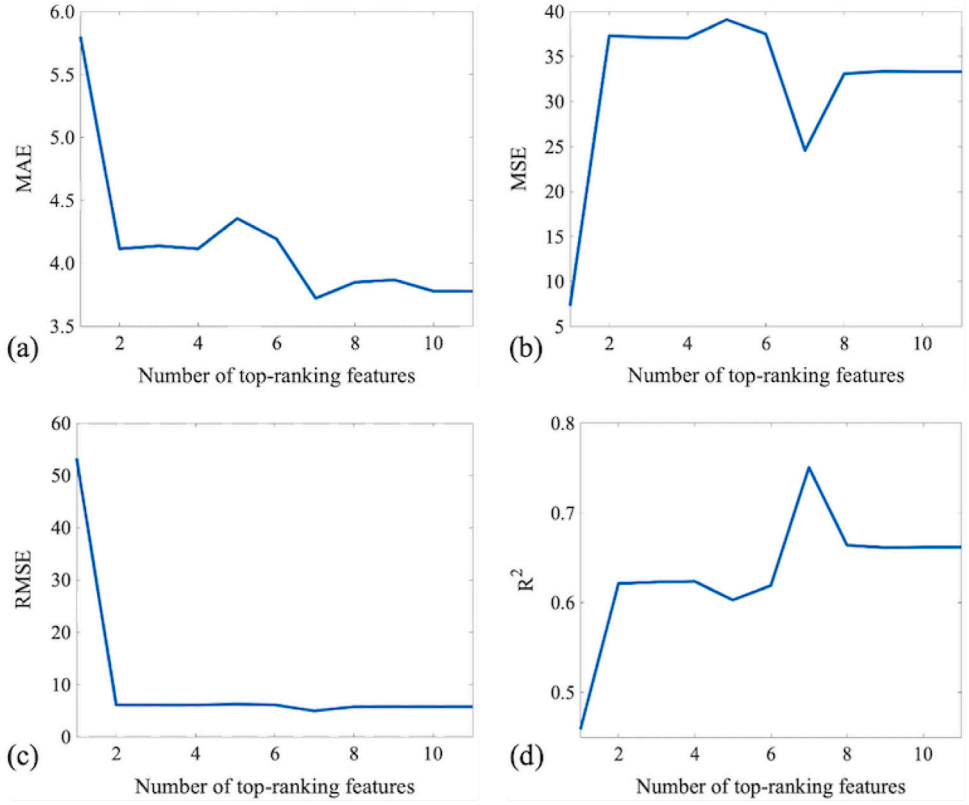

Fig. A.4. The performance of the LR model as a function of the number of top-ranking features evaluated by (a) MAE, (b) MSE, (c) RMSE, and (d) R-squared indices.

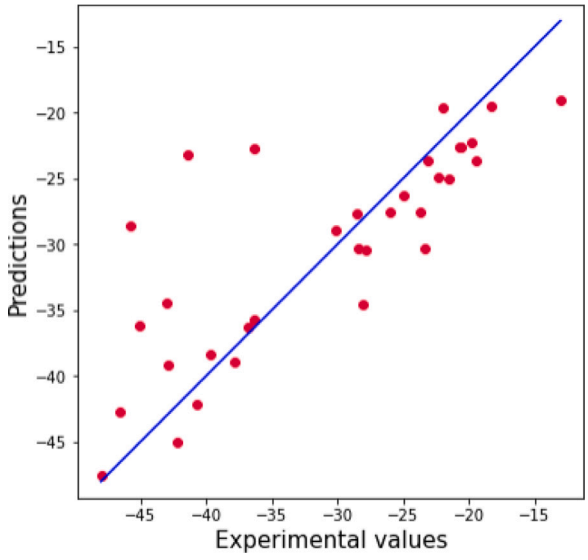

Fig. A.5. Actual values of experimental parabolic growth rate constants of high-temperature oxidation compared with values obtained from the LR model where it was trained with four top-ranking features and tested with 20% of the dataset (32 red dots).

References

[1] H. Abuluwefa, R. Guthrie, F. Ajersch, The effect of oxygen concentration on the oxidation of low-carbon steel in the temperature range 1000 to 1250°C, Oxid. Met. 46 (5) (1996) 423–440.

[2] L. Gong, N. Ruscassier, M. Ayouz, P. Haghi-Ashtiani, M.-L. Giorgi, Analytical model of selective external oxidation of Fe-Mn binary alloys during isothermal annealing treatment, Corros. Sci. 166 (2020) 108454.

[3] S. Aghaeian, W.G. Sloof, J.M.C. Mol, A.J. Böttger, Initial high-temperature oxidation behavior of Fe-Mn binaries in air: The kinetics and mechanism of oxidation, Oxid. Met. 98 (2022) 217–237.

[4] L. Gong, W. Jiang, D. Balloy, M.-L. Giorgi, Numerical model of selective external oxidation of Fe-Mn binary alloys during non-isothermal annealing treatment, Corros. Sci. 178 (2021) 108921.

[5] R. Pillai, A. Chyrkin, W.J. Quadakkers, Modeling in high-temperature corrosion: A review and outlook, Oxid. Met. 96 (5) (2021) 385–436.

[6] T. Nijdam, L. Jeurgens, W.G. Sloof, Modelling the thermal oxidation of ternary alloys—compositional changes in the alloy and the development of oxide phases, Acta Mater. 51 (18) (2003) 5295–5307.

[7] T. Nijdam, W.G. Sloof, Modelling of composition and phase changes in multiphase alloys due to growth of an oxide layer, Acta Mater. 56 (18) (2008) 4972–4983.

[8] S. Aghaeian, J. Brouwer, W. Sloof, J. Mol, A. Böttger, Numerical model for short-time high-temperature isothermal oxidation of Fe–Mn binaries at high oxygen partial pressure, High Temp. Corros. Mater. (2023) 1–18.

[9] R. Pillai, M. Romedenne, J. Peng, B. Pint, J.A. Haynes, G. Muralidharan, D. Shin, Lessons learned in employing data analytics to predict oxidation kinetics and spallation behavior of high-temperature NiCr-based alloys, Oxid. Met. 97 (1–2) (2022) 51–76.

[10] R. Ramprasad, R. Batra, G. Pilania, A. Mannodi-Kanakkithodi, C. Kim, Machine learning in materials informatics: recent applications and prospects, npj Comput. Mater. 3 (1) (2017) 1–13.

[11] J. Schmidt, M.R. Marques, S. Botti, M.A. Marques, Recent advances and applications of machine learning in solid-state materials science, npj Comput. Mater. 5 (1) (2019) 1–36.

[12] F.E. Bock, R.C. Aydin, C.J. Cyron, N. Huber, S.R. Kalidindi, B. Klusemann, A review of the application of machine learning and data mining approaches in continuum materials mechanics, Front. Mater. 6 (2019) 110.

[13] J. Peng, R. Pillai, M. Romedenne, B.A. Pint, G. Muralidharan, J. Allen Haynes, D. Shin, Data analytics approach to predict high-temperature cyclic oxidation kinetics of NiCr-based alloys, npj Mater. Degrad. 5 (1) (2021) 1–8.

[14] S.K. Bhattacharya, R. Sahara, T. Narushima, Predicting the parabolic rate constants of high-temperature oxidation of Ti alloys using machine learning, Oxid. Met. 94 (3) (2020) 205–218.

[15] C.D. Taylor, B.M. Tossey, High temperature oxidation of corrosion resistant alloys from machine learning, npj Mater. Degrad. 5 (1) (2021) 1–10.

[16] K. Pearson, A. Lee, On the laws of inheritance in man: I. Inheritance of physical characters, Biometrika 2 (4) (1903) 357–462.

[17] C. Giggins, F. Pettit, Oxidation of Ni-Cr alloys between 800° and 1200°C, Metall. Trans. 1 (4) (1970) 1088.

[18] G. Wallwork, The oxidation of alloys, Rep. Progr. Phys. 39 (5) (1976) 401.
[19] J.H. Friedman, Greedy function approximation: a gradient boosting machine, Ann. Statist. (2001) 1189–1232.
[20] M. Anirudh, M.S. Iyengar, P. Desik, M. Phaniraj, Artificial intelligence approach to predict elevated temperature cyclic oxidation of Fe-Cr and Fe-Cr-Ni alloys, Oxid. Met. (2022) 1–13.
[21] H. Bhadeshia, R. Dimitriu, S. Forsik, J. Pak, J. Ryu, Performance of neural networks in materials science, Mater. Sci. Technol. 25 (4) (2009) 504–510.
[22] B. Hkdh, Neural networks in materials science, ISIJ Int. 39 (10) (1999) 966–979.
[23] S.K. Dewangan, V. Kumar, Application of artificial neural network for prediction of high temperature oxidation behavior of AlCrFeMnNiW,X (x=0, 0.05, 0.1, 0.5) high entropy alloys, Int. J. Refract. Met. Hard Mater. 103 (2022) 105777.
[24] H.-S. Kim, S.-J. Park, S.-M. Seo, Y.-S. Yoo, H.-W. Jeong, H. Jang, Regression analysis of high-temperature oxidation of Ni-based superalloys using artificial neural network, Corros. Sci. 180 (2021) 109207.
[25] D.W. Yun, S. Seo, H. Jeong, I. Kim, Y. Yoo, Modelling high temperature oxidation behaviour of Ni-Cr-W-Mo alloys with Bayesian neural network, J. Alloys Compd. 587 (2014) 105–112.
[26] N. Islam, W. Huang, H.L. Zhuang, Machine learning for phase selection in multi-principal element alloys, Comput. Mater. Sci. 150 (2018) 230–235.
[27] S.K. Dewangan, S. Samal, V. Kumar, Microstructure exploration and an artificial neural network approach for hardness prediction in AlCrFeMnNiW,X high-entropy alloys, J. Alloys Compd. 823 (2020) 153766.
[28] A. Marasco, D. Young, The oxidation of iron-chromium-manganese alloys at 900°C, Oxid. Met. 36 (1) (1991) 157–174.
[29] P. Jackson, G. Wallwork, The oxidation of binary iron-manganese alloys, Oxid. Met. 20 (1) (1983) 1–17.
[30] P.A. Munther, J.G. Lenard, The effect of scaling on interfacial friction in hot rolling of steels, J. Mater Process. Technol. 88 (1–3) (1999) 105–113.
[31] K. Sachs, C. Tuck, Scale growth during Re-heating cycles, Mater. Corros. 21 (11) (1970) 945–954.
[32] R.Y. Chen, W. Yuen, The effects of steel composition on the oxidation kinetics, scale structure, and scale-steel interface adherence of low and ultra-low carbon steels, in: Materials Science Forum, Vol. 522, Trans Tech Publ, 2006, pp. 451–460.
[33] S. Chandra-ambhorn, T. Thublaor, P. Wiman, High temperature oxidation of AISI 430 stainless steel in Ar-H2O at 800°C, Corros. Sci. 167 (2020) 108489.
[34] D.J. Young, H. Yin, Water vapour effects on FeO scale growth: differences between iron and steel, Oxid. Met. 79 (5) (2013) 445–460.
[35] T. Zheng, J.T. Han, High temperature oxidation behavior of SUS310S austenitic stainless steel, in: Advanced Materials Research, Vol. 941, Trans Tech Publ, 2014, pp. 212–215.
[36] L. Cheng, B. Sun, C. Du, W. Gao, G. Cao, High-temperature oxidation behavior of Fe-10Cr steel under different atmospheres, Materials 14 (13) (2021) 3453.
[37] M. Hao, B. Sun, H. Wang, High-temperature oxidation behavior of Fe-1Cr-0.2Si Steel, Materials 13 (3) (2020) 509.
[38] D. Zou, Y. Zhou, X. Zhang, W. Zhang, Y. Han, High temperature oxidation behavior of a high Al-containing ferritic heat-resistant stainless steel, Mater. Charact. 136 (2018) 435–443.
[39] Y. Xu, X. Zhang, L. Fan, J. Li, X. Yu, X. Xiao, L. Jiang, Improved oxidation resistance of 15 wt.% Cr ferritic stainless steels containing 0.08-2.45 wt.% Al at 1000°C in air, Corros. Sci. 100 (2015) 311–321.
[40] A.M. Huntz, A. Reckmann, C. Haut, C. Sévérac, M. Herbst, F.C.T. Resende, A.C.S. Sabioni, Oxidation of AISI 304 and AISI 439 stainless steels, Mater. Sci. Eng. A 447 (1–2) (2007) 266–276.
[41] A.C.S. Sabioni, E.A. Malheiros, V. Ji, F. Jomard, W.A. de Almeida Macedo, P.L. Gastelois, Ion diffusion study in the oxide layers due to oxidation of AISI 439 ferritic stainless steel, Oxid. Met. 81 (3) (2014) 407–419.
[42] Y. Zhang, D. Zou, X. Wang, Q. Wang, R. Xu, W. Zhang, Influences of Si content on the high-temperature oxidation behavior of X10CrAlSi18 ferritic heat-resistant stainless steel at 700°C and 800°C, Surf. Coat. Technol. 422 (2021) 127523.
[43] Q. Shi, J. Liu, W. Wang, W. Yan, Y. Shan, K. Yang, High temperature oxidation behavior of SIMP steel, Oxid. Met. 83 (5) (2015) 521–532.
[44] Q. Gao, Z. Liu, H. Li, H. Zhang, C. Jiang, A. Hao, F. Qu, X. Lin, High-temperature oxidation behavior of modified 4Al alumina-forming austenitic steel: Effect of cold rolling, J. Mater. Sci. Technol. 68 (2021) 91–102.
[45] J. Wang, Y. Qiao, N. Dong, X. Fang, X. Quan, Y. Cui, P. Han, The influence of temperature on the oxidation mechanism in air of HR3C and aluminum-containing 22Cr-25Ni austenitic stainless steels, Oxid. Met. 89 (5) (2018) 713–730.
[46] T. Balaško, B. Šetina Batič, J. Medved, J. Burja, High-temperature oxidation behaviour of duplex Fe-Mn-Al-Ni-C lightweight steel, Crystals 12 (7) (2022) 957.
[47] R. Wang, M.J. Straszheim, R.A. Rapp, A high-temperature oxidation-resistant Fe-Mn-Al-Ni-Si alloy, Oxid. Met. 21 (1) (1984) 71–79.
[48] C. Kao, C. Wan, Effect of manganese on the oxidation of Fe-Mn-Al-C alloys, J. Mater. Sci. 23 (2) (1988) 744–752.
[49] R. Spotorno, High-temperature oxidation of AISI441 ferritic stainless steel for solid oxide fuel cells, in: Materials Science Forum, Vol. 1016, Trans Tech Publ, 2021, pp. 1381–1385.
[50] J.-Y. Yun, S.-A. Ha, C.-Y. Kang, J.-P. Wang, Oxidation behavior of low carbon steel at elevated temperature in oxygen and water vapor, Steel Res. Int. 84 (12) (2013) 1252–1257.
[51] J. Von Fraunhofer, G. Pickup, The oxidation behaviour of low alloy steels—Part1, Anti-Corros. Methods Mater. (1970).
[52] I. Kim, W. Cho, H. Kim, High-temperature oxidation of Fe3Al containing yttrium, J. Mater. Sci. 35 (18) (2000) 4695–4703.
[53] V. Bongiorno, R. Spotorno, D. Paravidino, P. Piccardo, On the high-temperature oxidation and area specific resistance of new commercial ferritic stainless steels, Metals 11 (3) (2021) 405.
[54] B. Talic, V. Venkatachalam, P.V. Hendriksen, R. Kiebach, Comparison of MnCo2O4 coated Crofer 22 H, 441, 430 as interconnects for intermediate-temperature solid oxide fuel cell stacks, J. Alloys Compd. 821 (2020) 153229.
[55] T. Brylewski, M. Nanko, T. Maruyama, K. Przybylski, Application of Fe-16Cr ferritic alloy to interconnector for a solid oxide fuel cell, Solid State Ion. 143 (2) (2001) 131–150.
[56] B. Talic, H. Falk-Windisch, V. Venkatachalam, P.V. Hendriksen, K. Wiik, H.L. Lein, Effect of coating density on oxidation resistance and Cr vaporization from solid oxide fuel cell interconnects, J. Power Sources 354 (2017) 57–67.
[57] D.J. Young, High Temperature Oxidation and Corrosion of Metals, Vol. 1, Elsevier, Amsterdam, 2008.
[58] T.K. Ho, The random subspace method for constructing decision forests, IEEE Trans. Pattern Anal. Mach. Intell. 20 (8) (1998) 832–844.
[59] N.S. Altman, An introduction to kernel and nearest-neighbor nonparametric regression, Amer. Statist. 46 (3) (1992) 175–185.
[60] M. Awad, R. Khanna, Efficient Learning Machines: Theories, Concepts, and Applications for Engineers and System Designers, Springer nature, 2015.
[61] F. Pedregosa, G. Varoquaux, A. Gramfort, V. Michel, B. Thirion, O. Grisel, M. Blondel, P. Prettenhofer, R. Weiss, V. Dubourg, et al., Scikit-learn: Machine learning in Python, J. Mach. Learn. Res. 12 (2011) 2825–2830.
[62] M. Abadi, P. Barham, J. Chen, Z. Chen, A. Davis, J. Dean, M. Devin, S. Ghemawat, G. Irving, M. Isard, et al., *TensorFlow*: A system for *Large* – *Scale* zrning, in: 12th USENIX Symposium on Operating Systems Design and Implementation, OSDI 16, 2016, pp. 265–283.
[63] D.A. Freedman, Statistical Models: Theory and Practice, Cambridge University Press, 2009.
[64] D. Chicco, M.J. Warrens, G. Jurman, The coefficient of determination R-squared is more informative than SMAPE, MAE, MAPE, MSE and RMSE in regression analysis evaluation, PeerJ Comput. Sci. 7 (2021) e623.
[65] H. Mehtani, M. Khan, B.N. Jaya, S. Parida, M. Prasad, I. Samajdar, The oxidation behavior of iron-chromium alloys: The defining role of substrate chemistry on kinetics, microstructure and mechanical properties of the oxide scale, J. Alloys Compd. 871 (2021) 159583.
[66] G.H. Meier, K. Jung, N. Mu, N.M. Yanar, F.S. Pettit, J. Pirón Abellán, T. Olszewski, L. Nieto Hierro, W.J. Quadakkers, G.R. Holcomb, Effect of alloy composition and exposure conditions on the selective oxidation behavior of ferritic Fe-Cr and Fe-Cr-X alloys, Oxid. Met. 74 (5) (2010) 319–340.
[67] J. Croll, G. Wallwork, The high-temperature oxidation of iron-chromium-nickel alloys containing 0–30% chromium, Oxid. Met. 4 (3) (1972) 121–140.
[68] H. Yin, S. Chan, W. Yuen, D. Young, Temperature effects on the oxidation of low carbon steel in N2-H2-H2O at 800–1200°C, Oxid. Met. 77 (5) (2012) 305–323.
[69] K. Chandra, A. Kranzmann, R. Saliwan Neumann, G. Oder, F. Rizzo, High temperature oxidation behavior of 9–12% Cr ferritic/martensitic steels in a simulated dry oxyfuel environment, Oxid. Met. 83 (2015) 291–316.
[70] D.P. Kingma, J. Ba, Adam: A method for stochastic optimization, 2014, arXiv preprint arXiv:1412.6980.
[71] I.N. Da Silva, D.H. Spatti, R.A. Flauzino, L.H.B. Liboni, S.F. dos Reis Alves, Artificial neural networks, Vol. 39, 39, Springer International Publishing, Cham, 2017.